Characterization of the New Vertical Neutron Camera Designed for the Low Neutron Emission Rate Plasma in Large Helical Device

Siriyaporn SANGAROON[1,2], Kunihiro OGAWA[1,3], Mitsutaka ISOBE[1,3], Yutaka FUJIWARA[1], Hiroyuki YAMAGUCHI[1], Shuji KAMIO[1], Ryosuke SEKI[1,3], Hideo NUGA[1], Makoto I. KOBAYASHI[1,3] and Masaki OSAKABE[1,3]

[1)]*National Institute for Fusion Science, National Institutes of Natural Sciences, Toki 509-5292, Japan*
[2)]*Department of Physics, Faculty of Science, Mahasarakham University, Maha Sarakham, Thailand*
[3)]*The Graduate University for Advanced Studies, SOKENDAI, Toki 509-5292, Japan*

(Received 22 December 2020 / Accepted 3 February 2021)

Characteristics of the new vertical neutron camera (VNC3) installed for the study of energetic-particle transport in the relatively low neutron emission rate (S_n) in Large Helical Device (LHD) deuterium plasma is investigated. Dependence of signal of VNC3 operating with the current mode on S_n shows that accurate neutron signal is obtained using VNC3 in low S_n range with 10 ms time bin where the error of neutron counts of first vertical neutron camera (VNC1) operating with the pulse counting mode is significantly large. Time-resolved measurements of neutron emission profiles in deuterium beam heated low S_n plasmas are performed. Although the line-integrated neutron obtained by VNC3 is wider due to its larger inner diameter of the collimator compared to VNC1, the neutron profile measured by VNC3 is almost matched with the neutron profile measured by VNC1. The time-resolved neutron profile measurement in low S_n discharge with relatively short time period becomes possible using VNC3.

Keywords: LHD, vertical neutron camera, neutron emission profile, energetic particle

DOI: 10.1585/pfr.16.1402039

1. Introduction

A study of energetic particles (EPs) transport has been performed in existing magnetic confinement fusion devices to contribute to an understanding of the confinement of deuterium-tritium fusion born alpha particles in a fusion burning plasma [1]. In tokamaks, studies of EPs behaviors have been studied using the neutron diagnostics [2]. In particular, neutron cameras have played an important role in the understanding of radial transport of EPs in large tokamaks, e.g., TFTR [3, 4], JET [5, 6], and JT-60U [7, 8]. In ITER, neutron cameras having horizontal and vertical line of sight will be installed [9, 10]. In stellarators/helical devices, the study of EP confinement has been well advanced by starting the plasma experiment using deuterium gas since March 2017 in the Large Helical Device (LHD) using the comprehensive neutron diagnostics and intensive neutral beam (NB) injections [11–14]. To study the EP transport in helical devices, the first vertical neutron camera (the so-called VNC1) designed for working at total neutron emission rate (S_n) of 10^{16} order, which is the expected maximum S_n in LHD [15], has been working since 2017 [16, 17]. Studies of classical confinement as well as transport of EPs due to the energetic ion driven magnetohydrodynamic (MHD) instabilities have been reported using VNC1 [18–21]. In the plasma discharges, where the relatively strong MHD instabilities were observed, the time resolution of neutron emission profile was 10 ms with ∼10% error bar because of the relatively low neutron count due to the relatively low S_n of 10^{14} to 10^{15} n/s [21]. To study the EP transport with the higher time resolution in relatively low S_n discharges, the high detection efficiency vertical neutron cameras (the so-called VNC2 and the so-called VNC3) were developed and were used in LHD from 2018 [22, 23]. This paper is devoted to characterization of the VNC3 designed for the relatively low S_n discharges in LHD.

2. Experimental Setup

Figure 1 a) shows the top view of LHD, the arrangement of the two perpendicular NB injections (P-NB), the arrangement of the three tangential NB injections (N-NB), and the position of the three VNCs. In LHD, the direction of the toroidal magnetic field (B_T) can be operated by clockwise (CW) and counterclockwise directions viewing from the top. Here, the blue arrow indicates the direction of B_T that is CW direction used in the experiments. In this work, we only use N-NB#3 which injects NBs with the counter-directions in respect to B_T and mainly produces the counter-going transit EPs. The VNC1 is installed at the 2.5L LHD lower port [17]. The VNC2 and VNC3 are installed at the 1.5L LHD lower port to view in different

author's e-mail: sangaroon.siriyaporn@nifs.ac.jp

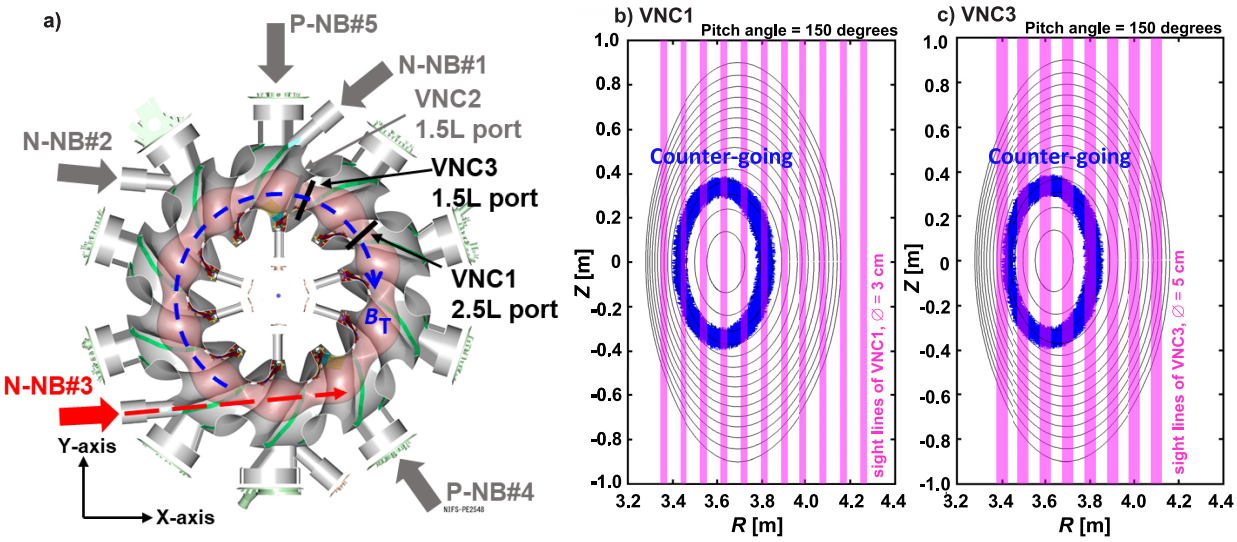

Fig. 1 a) A schematic top view of the LHD, the arrangement of the P-NBs and N-NBs, and the location of the VNCs. The blue arrow indicates the direction of the B_T. The sight lines of b) VNC1 and c) VNC3 as well as Poincaré plot of collisionless orbit of a counter-going transit beam ion are shown. The energy and the initial pitch angle of beam ion are 180 keV and 150 degrees, respectively. Here, the magnetic configuration is B_T of 2.75 T and R_{ax_vac} of 3.6 m.

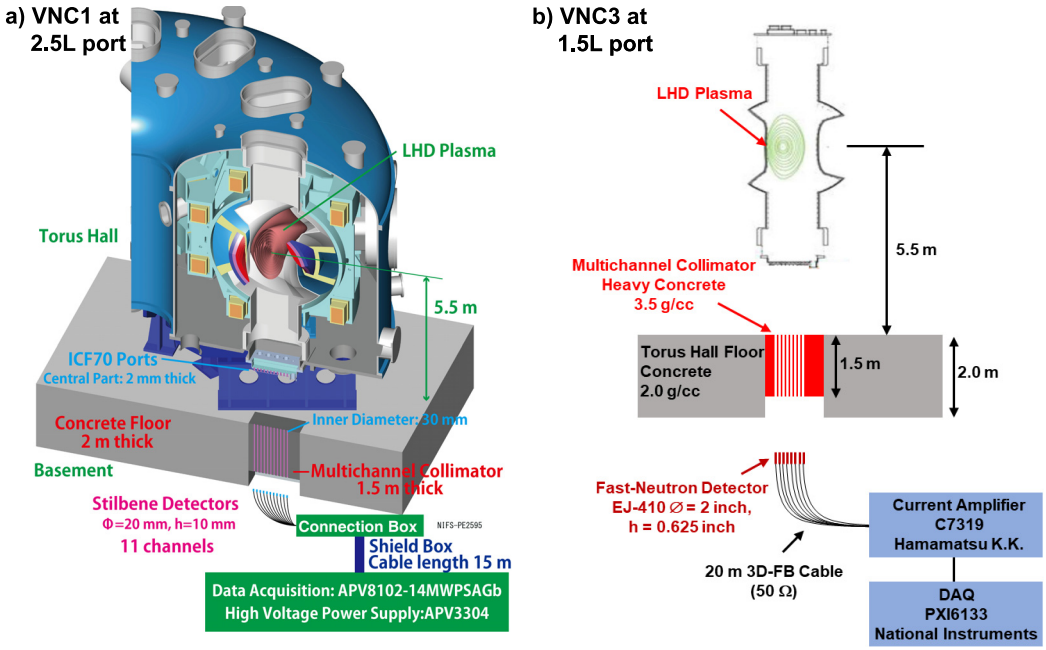

Fig. 2 a) A schematic drawing of the LHD cut view and the VNC1 operating with the pulse counting mode with n/γ discrimination capability [15]. b) A schematic of VNC3 operating with the current mode.

plasma cross-sections [22, 23]. Note that VNC2 is beyond the scope of this paper. The sight lines of VNC1 and VNC3 are shown in Figs. 1 b) and 1 c). In these figures, the typical orbit of a counter-going transit beam ion created by N-NB injection calculated by collisionless Lorentz orbit code (LORBIT) [24] is plotted. Here, B_T and magnetic axis position (R_{ax_vac}) are set to be 2.75 T and 3.6 m, respectively. The orbit is launched from radius (R) of 3.6 m and height from the midplane (Z) of 0.3 m, with the initial pitch angle of approximately 150 degrees. The initial energy is set to be 180 keV. Note that the typical Larmor radius evaluated by the energy is approximately 3.2 cm in this condition.

Figure 2 a) shows the schematic drawing of the LHD cut view and the schematic drawing of VNC1 operating with the pulse counting mode and characterized by the high counting rate capability in the range of ~MHz [17]. VNC1 has eleven sight lines. The sight lines are aligned radially at R of 3.36 m, 3.45 m, 3.54 m, 3.63 m, 3.72 m,

3.81 m, 3.90 m, 3.99 m, 4.08 m, 4.17 m, and 4.26 m. The inner diameter of each collimator pipe is 3 cm. The multichannel collimator with the 1.5 m thick hematite (Fe_2O_3)-doped heavy concrete is installed in the 2 m thick torus hall floor ordinary concrete at 2.5L LHD lower port. A stilbene crystal with a diameter of 2 cm and a height of 1 cm coupled with a high-gain stability photomultiplier tube (H11934-100-10MOD, Hamamatsu Photonics K.K. [25]) is used for VNC1. The stilbene detector has sensitivity to both fast-neutrons and γ-rays. The charge comparison method which exploits the different rise/decay times of neutron and γ-ray induced pulses is used. The signal of the stilbene detector is directly fed into the data acquisition system (DAQ), equipped with a 50 Ω/14 bit/1 GHz analog-to-digital converter (ADC) with a field programmable gate array and 1 GB of dynamic random-access memory (APV8102-14MWPSAGb, Techno AP Corp. [26]). The acquired data by the DAQ is transferred to the data acquisition PC which is connected to the LHD experimental database. VNC1 provides the neutron profile with the spatial resolution of ~7 cm in FWHM (Full Width at Half Maximum) at the midplane [27].

Figure 2 b) shows the schematic drawing of VNC3 operating with the current mode and characterized by high detection efficiency. The VNC3 has eight sight lines. The sight lines align radially at R of 3.4 m, 3.5 m, 3.6 m, 3.7 m, 3.8 m, 3.9 m, 4.0 m, and 4.1 m. The inner diameter of each collimator pipe is 5 cm. The multichannel collimator with the 1.5 m thick hematite (Fe_2O_3)-doped heavy concrete is installed in the 2 m thick torus hall floor ordinary concrete at 1.5L LHD lower port. The hematite-doped heavy concrete is used for VNC3 as that used for VNC1 due to the high capability to shield ambient neutron and γ-ray at the detector. An EJ-410 scintillator [28] with a diameter of 2 inches and a height of 0.625 inches coupled with the two-inches size photomultiplier (H7195, Hamamatsu Photonics K.K. [29]) is used for VNC3. EJ-410 is fast-neutron scintillator (energy of neutron $E_n > 1$ MeV) and has less sensitivity to γ-ray. In EJ410, the scintillation pulse generated by γ-ray is usually smaller than those generated by neutron. The signal from the detector is directly fed into the low input impedance current amplifier (C7319, Hamamatsu Photonics K.K. [30]) which has the frequency bandwidth of 20 kHz and the gain of 10^4. The output signal from the current amplifier is acquired by the ADC of 14 bit/±10 V with the sampling frequency of 1 MHz and the input impedance of 100 MΩ (PXI6133, National Instruments [31]). The data acquired by the ADC is transferred to the data acquisition PC which is connected to the LHD experimental database. The VNC3 provides the neutron profile with the spatial resolution of ~13 cm in FWHM at the midplane [23].

3. Experimental Results

3.1 Neutron measurement capability in low S_n region

The LHD deuterium plasma discharges in relatively low S_n range between ~3×10^{13} n/s and ~4×10^{14} n/s and in MHD-quiescent plasmas are performed in order to study the capability in neutron measurement of VNC1 and VNC3 by compared to the capability in neutron measurement of the high time resolution neutron flux monitor (NFM) [11, 32, 33]. In the experiments, R_{ax_vac} is set to be 3.6 m and B_T is set to be 2.75 T with CW directions viewed from the top. For all discharges, the N-NB#3 has been

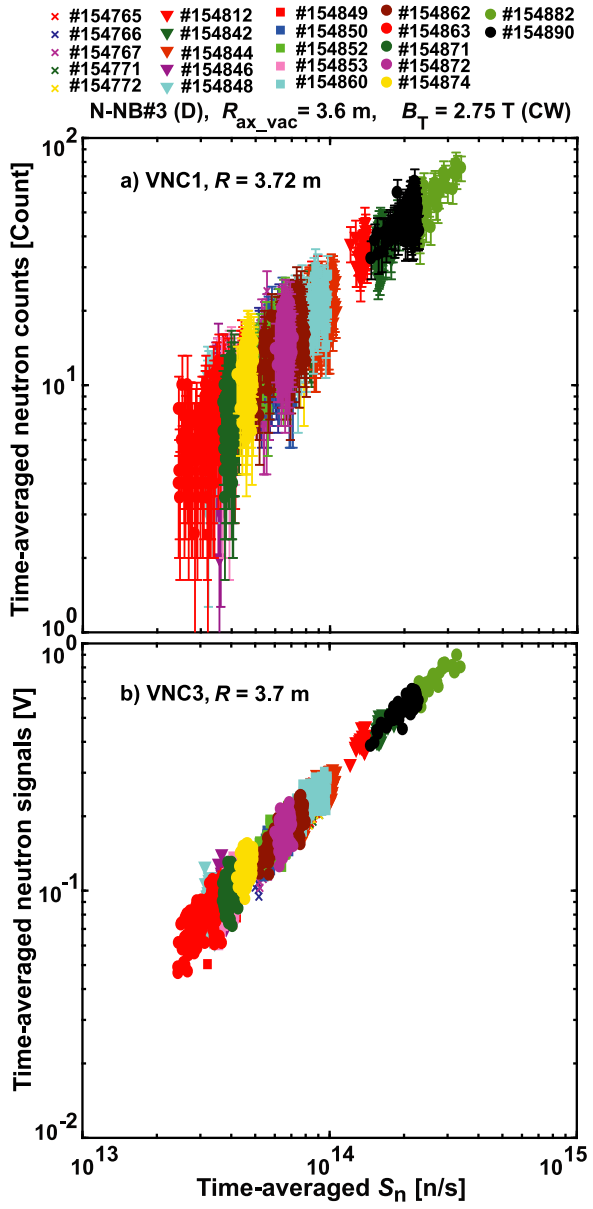

Fig. 3 a) Comparison of time-averaged neutron counts measured by VNC1 at R = 3.72 m and S_n measured by NFM. b) Comparison of time-averaged neutron signals measured by VNC3 at R = 3.7 m and S_n measured by NFM. Here, the time bin for time averaging is 10 ms.

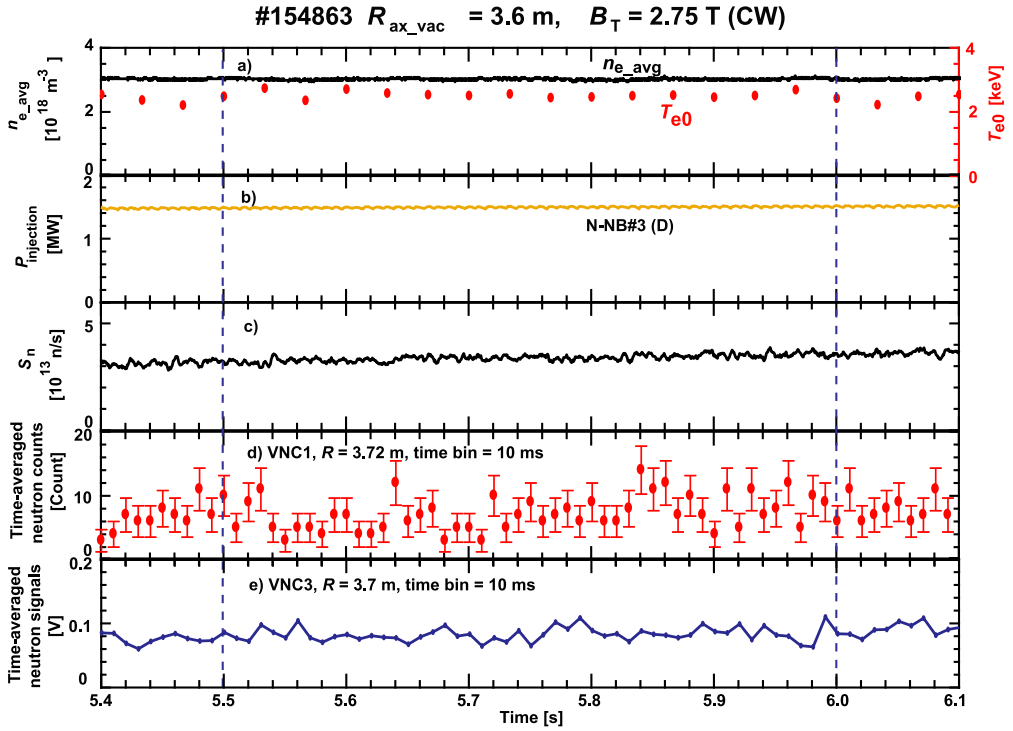

Fig. 4 Time evolution of relatively low S_n deuterium plasma discharge #154863. a) Line-averaged electron density n_{e_avg} and central electron temperature T_{e0}, b) injection power of N-NB#3 injected with the counter-direction, c) S_n measured by NFM, d) the time-averaged neutron counts measured by VNC1 at R of 3.72 m, and e) the time-averaged neutron signals measured by VNC3 at R of 3.70 m are shown. Time interval between 5.5 s and 6.0 s is selected for line-integrated neutron profiles study.

injected with the counter-direction in respect to B_T. Figure 3 a) shows the dependence of time-averaged neutron counts measured by VNC1 at R = 3.72 m on S_n measured by the NFM. Here, the vertical error bar comes from the standard deviation of counts with the Poisson distribution $\sigma = \sqrt{\text{neutron counts}}$. The time bin for the time-averaged is 10 ms. In the relatively high S_n discharge, e.g., #154882, the obtained σ is between ~12% and ~16%, whereas, the obtained σ is between ~28% and ~63% in the relatively low S_n discharge, e.g., #154863. Figure 3 b) shows the dependence of time-averaged neutron signals measured by VNC3 at R = 3.7 m on S_n measured by NFM. Here, the time-averaged neutron signals are averaged from the measured voltage signals within 10 ms. Note that in the current mode, the signal is made of the overlapping of many pulses, therefore, the σ of the signals is not defined in VNC3 measurement. Hence, VNC1 provides the neutron counts with the relatively large error bar under the relatively low S_n condition with the 10 ms time bin, whereas under relatively low S_n condition with the 10 ms VNC3 can provide the neutron signal, as designed. Moreover, it is found that during the low neutron yield deuterium plasma, i.e., #154863, the fluctuation of the time-averaged S_n measured by NFM is approximately 10%, the fluctuation of the time-averaged neutron counts measured by VNC1 is approximately 28%, and the fluctuation of the time-averaged neutron signals measured by VNC3 is approximately 15%. Therefore, it is experimentally confirmed that VNC3 has the ability to measure accurate neutron signal in relatively low S_n discharges within 10 ms than VNC1 compared to the high time resolution NFM.

3.2 Measurement of the neutron emission profile in low S_n discharge

To compare the neutron emission measurement characteristics of VNC3 to VNC1, measurements of neutron profile in the relatively low S_n discharge and in MHD-quiescent plasma was performed. Figure 4 shows the time evolution of the relatively low S_n deuterium plasma discharge #154863. In this experiment, R_{ax_vac} and B_T are set to be 3.60 m and 2.75 T, respectively. Line-averaged electron density (n_{e_avg}) is ~3×10^{18} m^{-3}, and the central electron temperature (T_{e0}) is ~2.5 keV. N-NB#3 with the injection energy of ~170 keV and the injection power of ~1.5 MW is injected during the time interval between 5.5 s and 6.0 s. S_n measured by the NFM is ~3×10^{13} n/s. Figure 4 d) shows time-averaged neutron counts measured by VNC1 at R = 3.72 m with the vertical error bar of σ with time bin of 10 ms. The error bar of VNC1 is relatively large due to low neutron count because of low S_n condition. The discussion of time-resolved neutron emission changes within 10 ms seems to be difficult in this discharge using VNC1. Figure 4 e) shows time-averaged neutron signals measured by VNC3 at R = 3.7 m with time bin of 10 ms. Relatively smooth neutron signal of VNC3 as observed in low S_n condition is obtained as the result obtained by the

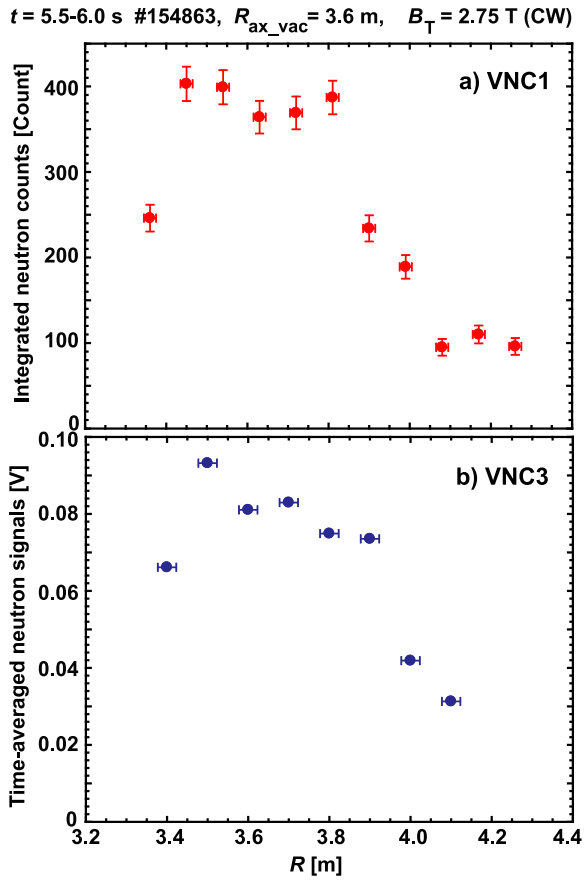

Fig. 5 The line-integrated neutron profiles of relatively low S_n deuterium plasma discharge #154863 during time interval of 5.5 s and 6.0 s measured by a) the VNC1 and b) the VNC3.

NFM.

The line-integrated neutron profiles measured by VNC1 and VNC3 in time interval between 5.5 s and 6.0 s as a function of R is shown in Fig. 5. Line-integrated neutron profile measured by VNC3 has a relatively broad profile as obtained in VNC1. The relatively broad neutron profile obtained in counter NB injection case is consistent with the neutron profile obtained in previous experiments with high B_T conditions [14]. Relatively high neutron count region appears in R of 3.45 m to 3.8 m for VNC1, whereas for VNC3 relatively high neutron signal region appears in R of 3.5 m to 3.9 m. The σ of line-integrated neutron profile measured by VNC1 is approximately 5% in the relatively high neutron counts region. Although the relatively wide profile is observed in VNC3 compared to VNC1 due to the larger inner diameter of the collimator, the neutron emission profile measured by VNC3 is almost matched with the neutron emission profile measured by VNC1.

4. Summary

The characteristics of VNC3 operating with the current mode were investigated and were compared to VNC1 operating with the pulse counting mode in low S_n discharges. Dependence of VNC3 signal on S_n shows that VNC3 can be used in relatively low S_n discharge with 10 ms time resolution, where the statistical error of neutron counts is relatively large in VNC1 measurement. The line-integrated neutron profiles in the counter-NB injection was measured by VNC3 and obtained neutron profile was compared to VNC1. The line-integrated neutron profile measured by VNC3 is consistent with the profile obtained by VNC1. It is clearly shown that the neutron profile measurement in low S_n discharge with relatively short time period becomes possible by means of VNC3.

Acknowledgments

This research was partly supported by NIFS Collaboration Research programs (KOAH037), by the LHD project budget (ULHH034 and ULGG801), and by the NINS program of Promoting Research by Networking among Institutions (Grant Number 01411702). We are pleased to acknowledge the assistance of LHD Experiment Group.

[1] A. Fasoli *et al.*, Nucl. Fusion **47**, S264 (2007).
[2] O.N. Jarvis, Plasma Phys. Control. Fusion **36**, 209 (1994).
[3] A.L. Roquemore *et al.*, Rev. Sci. Instrum. **61**, 3163 (1990).
[4] A.L. Roquemore *et al.*, Rev. Sci. Instrum. **68**, 544 (1997).
[5] J.M. Adams *et al.*, Nucl. Instrum. Methods Phys. A **329**, 277 (1993).
[6] O.N. Jarvis *et al.*, Fusion Eng. Des. **34-35**, 59 (1997).
[7] M. Ishikawa *et al.*, Rev. Sci. Instrum. **73**, 4237 (2002).
[8] M. Ishikawa *et al.*, Rev. Sci. Instrum. **77**, 10E706 (2006).
[9] F.B. Marcus *et al.*, Rev. Sci. Instrum. **68**, 514 (1997).
[10] D. Marocco *et al.*, J. Instrum. **7**, C03033 (2012).
[11] M. Isobe *et al.*, IEEE Trans. Plasma Sci. **46**, 2050 (2018).
[12] K. Ogawa *et al.*, Nucl. Fusion **59**, 076017 (2019).
[13] M. Isobe *et al.*, Nucl. Fusion **58**, 082004 (2018).
[14] K. Ogawa *et al.*, Plasma Fusion Res. **16**, 1102023 (2021).
[15] M. Osakabe *et al.*, Fusion Sci. Technol. **72**, 199 (2017).
[16] K. Ogawa *et al.*, Rev. Sci. Instrum. **85**, 11E110 (2014).
[17] K. Ogawa *et al.*, Rev. Sci. Instrum. **89**, 113509 (2018).
[18] H. Kawase *et al.*, Plasma Fusion Res. **13**, 3402122 (2018).
[19] K. Ogawa *et al.*, submitted to Plasma Phys. Control. Fusion.
[20] K. Ogawa *et al.*, Nucl. Fusion **58**, 044001 (2018).
[21] K. Ogawa *et al.*, Plasma Phys. Control. Fusion **60**, 044005 (2018).
[22] K. Ogawa *et al.*, Nucl. Fusion **60**, 112011 (2020).
[23] S. Sangaroon *et al.*, Rev. Sci. Instrum. **91**, 083505 (2020).
[24] M. Isobe *et al.*, J. Plasma Fusion Res. SERIES **8**, 330 (2009).
[25] H11934-100-10MOD, Hamamatsu Photonics K.K. (https://www.hamamatsu.com/resources/pdf/etd/R11265U_H11934_TPMH1336E.pdf).
[26] APV8102-14MWPSAGb, Techno AP Corp. (http://www.technoap.com/img/APV8102_14MWPSAGb.pdf).
[27] T. Nishitani *et al.*, Fusion Eng. Des. **123**, 1020 (2017).
[28] EJ-410 scintillator (https://eljentechnology.com/products/neutron-detectors/ej-410).
[29] H7195, Hamamatsu Photonics K.K. (https://www.hamamatsu.com/resources/pdf/etd/High_energy_PMT_

TPMZ0003E.pdf).
[30] C7319, Hamamatsu Photonics K.K. (https://s1.dtsheet.com/store/data/000749671.pdf?key=2f4cb749296cb6e8895ac79f7a1c378a&r=1).
[31] PXI6133, National Instruments (https://www.ni.com/pdf/manuals/371231d.pdf).
[32] M. Isobe *et al.*, Rev. Sci. Instrum. **85**, 11E114 (2014).
[33] D. Ito *et al.*, Plasma Fusion Res. **16**, 1405018 (2021).